

Impact of the top silicon thickness on phonon-limited electron mobility in (110)-oriented ultrathin-body silicon-on-insulator *n*-metal-oxide-semiconductor field-effect transistors

Hui-Chang Moon, Seong-Je Kim, Tae-Hun Shim, and Jea-Gun Park^{a)}

Department of Electronics and Computer Engineering, Hanyang University, 17 Haengdang-Dong, Seongdong-Gu, Seoul 133-791, Korea

(Received 2 July 2007; accepted 2 August 2007; published online 25 September 2007)

We investigated through a theoretical simulation how the phonon-limited electron mobility in both (110)- and (100)-oriented ultrathin-body (UTB) silicon-on-insulator (SOI) *n*-metal-oxide-semiconductor field-effect transistors (MOSFETs) depends on the top silicon thickness within a range from 20 to 2 nm. No electron mobility enhancement was observed in (110) UTB SOI *n*-MOSFETs when the top silicon thickness was around 5 nm, unlike in (100) UTB *n*-MOSFETs. Thus, electron mobility in (110) UTB SOI *n*-MOSFETs decreased with top silicon thickness, particularly in the range below 10 nm. We attributed the electron mobility degradation in (110) UTB SOI *n*-MOSFETs within the top silicon thickness range below 10 nm to a decrease in the effective width of the inversion layer and an increase in intravalley acoustic phonon scattering, rather than to less carrier repopulation due to less band splitting between two- and fourfold valleys.

© 2007 American Institute of Physics. [DOI: [10.1063/1.2784079](https://doi.org/10.1063/1.2784079)]

I. INTRODUCTION

As the design rule for metal-oxide-semiconductor field-effect transistors (MOSFETs) decreases to below 50 nm, the fully depleted silicon-on-insulator (SOI) MOSFET fabricated on an ultrathin body (UTB) has become a candidate device structure because of its suppression of the short-channel effect and its high-speed performance.^{1,2} In conventional bulk MOSFETs, the doping concentration in the channel has to be increased to reduce short-channel effects. This, however, increases impurity scattering, resulting in mobility degradation.³ In contrast, the UTB SOI MOSFET has attractive properties, such as no punch-through path between source and drain and suppression of the short-channel effect. In addition, the off-leakage current is low and the subthreshold swing is independent of the substrate doping concentration in UTB SOI MOSFETs.⁴ Consequently, a high doping concentration is not necessary in UTB SOI *n*-MOSFETs. Furthermore, it has been reported that mobility in an inversion layer can be increased by decreasing the top silicon thickness (T_{Si}) because of the subband modulation effect.^{5,6}

In complementary MOS (CMOS) technologies, the imbalance of the current drivability between *n*- and *p*-MOSFETs needs to be suppressed to achieve high device performance. From this viewpoint, the mobility is an important parameter through which we can determine the current drivability. Many researchers have studied mobility-enhancement technologies such as substrate strain,⁷⁻⁹ the hybrid substrate,¹⁰ Ge channel,¹¹ and process-induced strain.^{12,13} For the silicon orientation effect, low electron mobility on a (110) surface is an obstacle in high performance CMOS devices because the electron mobility on a (110) surface is lower than that on a (100) surface; otherwise, the hole

mobility on the (100) surface is lower than that on the (110) surface. Recent experimental results have shown that there is no electron mobility enhancement in (110) UTB SOI *n*-MOSFETs within a top silicon thickness range of 10 nm.¹⁴ However, this phenomenon in (110) UTB SOI *n*-MOSFETs has not been reviewed theoretically in detail. Therefore, we have investigated the electron mobility behavior in (110) UTB SOI *n*-MOSFETs having sub-20-nm top silicon thickness through a theoretical simulation in order to understand the physical mechanism underlying this phenomenon.

II. SIMULATION METHOD

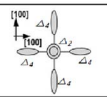
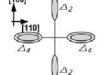
We assumed that the channel electron could be referred to as a two-dimensional electron gas (2DEG) on (110) UTB *n*-MOSFETs. In the bulk Si, the constant-energy surface of an electron is a set of six spheroids, which are called valleys, directed to six $\langle 100 \rangle$ orientations in the momentum space. When the orientation of the surface is given, six valleys are projected onto the specific plane because the inversion-layer electrons are modeled as a 2DEG.¹⁵ On the surface, the equivalent valleys can be classified into two types, such as two- and fourfold valleys. The effective mass of an electron in silicon depends on the surface orientation. The effective mass and band structure of each valley are summarized in Table I.

To determine the subband energy and envelope wave functions in each valley, Schrodinger equations of two- and fourfold valleys were calculated separately using two equations,

$$-\frac{\hbar^2}{2m_z} \frac{d^2}{dz^2} \psi_i(z) - q\Phi(z) \psi_i(z) = E_i \psi_i(z), \quad (2.1)$$

^{a)}Electronic mail: parkjgl@hanyang.ac.kr

TABLE I. Effective mass and subband structure. m_z , m_D , and m_c are out-of-plane effective mass, density-of-state effective mass, and conductivity effective mass, respectively.

effective orientation	m_z		m_D		m_c		2D subband structure
	2-fold	4-fold	2-fold	4-fold	2-fold	4-fold	
(100)	0.916	0.19	0.19	0.417	0.19	0.315	
(110)	0.19	0.315	0.417	0.324	0.315	0.283	

$$-\frac{\hbar^2}{2m_{z4}} \frac{d^2}{dz^2} \psi_i(z) - q\Phi(z)\psi_i'(z) = E_i' \psi_i'(z), \quad (2.2)$$

where m_{z2} and m_{z4} are the out-of-plane effective masses in a two- and a fourfold valley, respectively, E_i and ψ_i are the i th subband energy and envelope wave function in a twofold valley, E_i' and ψ_i' are the i th subband energy and envelope wave function in a fourfold valley, and $\Phi(z)$ is a potential energy obtained through device simulation [Silvaco ATLAS (Ref. 16)]. The subband energy of a two- and a fourfold valley, E_i and E_i' , depends on the out-of-plane mass (m_z). For the (110) surface, the lowest subband energy of the fourfold valley, E_0' , is lower than that of the twofold valley, E_0 , in contrast to the (100) surface, since the out-of-plane normal effective mass (m_z) of the fourfold valley is greater than that of the twofold valley.¹⁷ Note that the higher m_z provides lower subband energy. Therefore, the low valley in the (110) plane and the (100) plane is a fourfold valley and a twofold valley, respectively. Since phonon scattering is not only the main scattering mechanism for inversion-layer electron mobility but also independent of the process,^{6,18} we considered only the phonon scattering from among the various scattering mechanisms. The phonon-limited electron mobility was obtained through the relaxation time approximation (RTA). The subband energy and envelope wave function of each valley on both the (110) and the (100) surfaces were included. Figure 1 illustrates the schematic scattering process and transition path between valleys (e.g., from a twofold valley to two- or fourfold valley, and from a fourfold valley

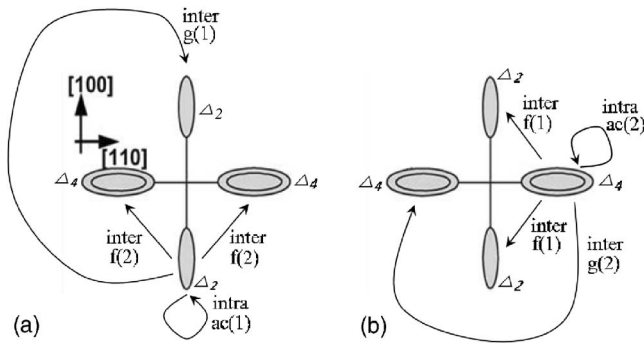


FIG. 1. Scattering diagrams for (110) surface: (a) scattering process from twofold valley and (b) scattering process from fourfold valley, where Δ_2 and Δ_4 denote the two- and fourfold valley, respectively. The number in each set of parentheses is the degeneracy number in each scattering process. Intra-ac is acoustic phonon scattering, and inter-f and inter-g are intervalley f-type phonon scattering and g-type phonon scattering, respectively.

TABLE II. Physical and scattering parameters.

Physical parameters		
m_0	Free electron mass	$9.109\,382\,6 \times 10^{-31}$ kg
k_B	Boltzmann constant	$1.380\,650\,5 \times 10^{-23}$ J/K
q	Elementary charge	$1.602\,176\,53 \times 10^{-19}$ C
\hbar	Planck constant over 2π	$1.054\,571\,68 \times 10^{-34}$ J s
ρ	Crystal density	2329 kg/m ³
s_l	Sound velocity	9037 m/s
Scattering parameters		
D_{ac}	Acoustic deformation potential	12 eV
E_{fp}	f-type phonon energy	59.0 meV
D_{fp}	f-type phonon deformation potential	1.1×10^9 eV/cm
E_{gp}	g-type phonon energy	63.0 meV
D_{gp}	g-type phonon deformation potential	4.0×10^8 eV/cm

to a two- or fourfold valley) in a (110) surface. Since the subband structure in the plane differs between the (110) surface and the (100) surface, the scattering process degeneracy on a (110) surface is also dissimilar to that on a (100) surface.¹⁸ The physical and simulation parameters are summarized in Table II. In our simulation, the two- and the fourfold-valley electron mobility were calculated separately, and the electron occupancy in each subband was summed to determine the total electron mobility. The lowest three subbands were considered. The substrate doping concentration was 7.0×10^{15} cm⁻³, and the temperature was fixed at room temperature.

III. RESULTS AND DISCUSSION

We investigated the dependence of the electron mobility on crystal orientation for UTB SOI n -MOSFETs. Figure 2 shows the calculated phonon-limited electron mobility in both (110) and (100) n -MOSFETs as a function of top silicon thickness. For the (110) UTB n -MOSFETs, no mobility enhancement within a silicon thickness range of approximately less than 5 nm was observed, in contrast to that observed for the (100) UTB n -MOSFETs. Particularly, the electron mobility of the (110) UTB SOI n -MOSFETs decreased with the top silicon thickness more significantly than that of the (100) UTB n -MOSFETs. It has been reported that the subband energy split increases with decreasing top silicon thickness,

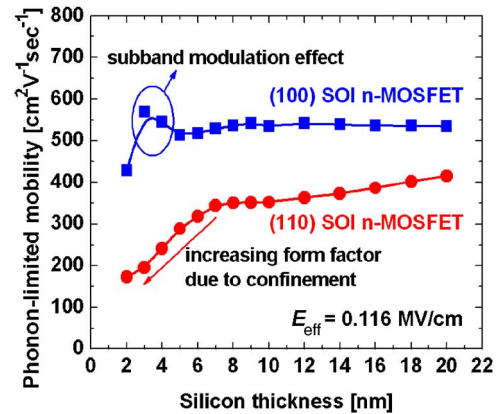


FIG. 2. (Color online) Phonon-limited electron mobility as a function of top silicon thickness.

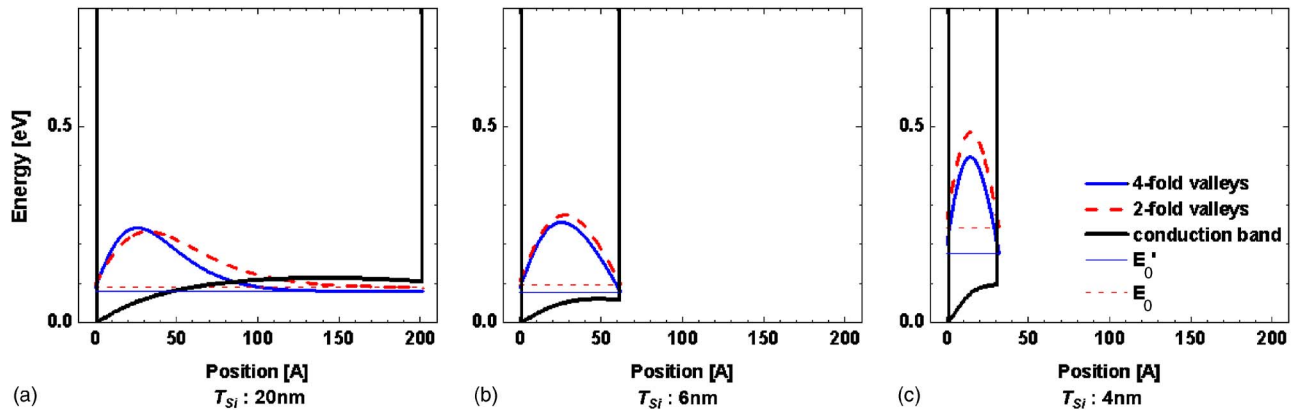


FIG. 3. (Color online) Diagrams of wave function and subband energy for the top silicon thickness from 20 nm (a) to 4 nm (c) in (110) UTB SOI *n*-MOSFETs, where E_0 and E'_0 are the lowest subband energy for two- and fourfold valleys, respectively.

resulting in enhanced mobility at a top silicon thickness of about 5 nm in (100) UTB SOI.⁶ In (110) *n*-MOSFETs, however, as the top silicon becomes thinner, the electron mobility decreases (Fig. 2). This is related to the envelope wave functions, ψ_i and ψ'_i , being confined in an ultrathin top silicon thickness of less than 10 nm, and it makes the band split between the two- and fourfold valleys bigger. Figure 3 shows that the envelope wave functions and subband energy of a (110) SOI *n*-MOSFET in each valley as a function of the top silicon thickness, i.e., at 20, 6, and 4 nm. The subband energy in each valley increases with decreasing top silicon thickness. The increment of the energy in the twofold valley, which is a high valley in the (110) surface, is greater than that of the energy in the fourfold valley, which is a low valley in (110), as a result of the difference in out-of-plane effective mass (m_z) between two- and fourfold valleys. In addition, the heavy m_z results in a strong rise in the subband energy.

Figure 4 shows the lowest subband energy difference (ΔE_0) as a function of the top silicon thickness in both the (110) and (100) surfaces. The ΔE_0 of the (110) and (100) surfaces is E_0 (subband energy at the twofold valley) minus E'_0 (subband energy at the fourfold valley) and E'_0 minus E_0 , respectively, because the low valley of the (110) surface is a fourfold valley while that of the (100) surface is a twofold

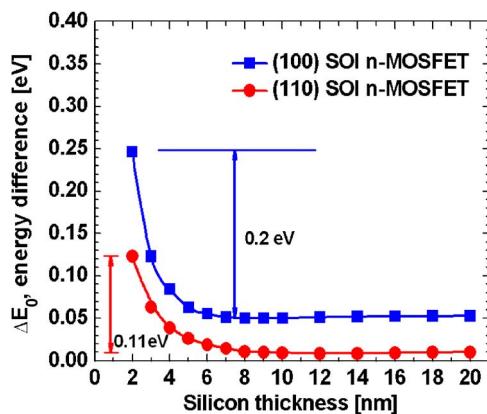


FIG. 4. (Color online) The lowest subband energy difference (ΔE_0) in both (110) and (100) surfaces as a function of top silicon thickness in UTB SOI *n*-MOSFETs.

valley. The ΔE_0 of the (110) surface was smaller than that of the (100) surface due to a smaller m_z difference in the (110) surface than in the (100) surface—the m_z difference in the (110) surface is $0.125m_0$ (0.315 for fourfold and 0.19 for twofold valleys), whereas that in the (100) surface is $0.726m_0$ (0.916 for twofold and 0.19 for fourfold valleys). In the top silicon thickness range from 6 to 4 nm, the subband energy difference in both the (110) and (100) surfaces increased abruptly with a decrease in the top silicon thickness; this was because of subband modulation.⁶ The subband energy split makes it possible to reduce intervalley phonon scattering. However, since the subband energy difference of the (110) surface was as low as approximately half of that for the (100) surface, indicating a lower energy split in (110) than in (100), the intervalley phonon scattering rate in the (110) surface is less than that in the (100) surface. As a result, it is difficult to enhance the electron mobility in (110)-oriented UTB SOI *n*-MOSFETs.

In addition, the subband energy split leads to repopulation of the electrons. The electron concentrations in each valley were calculated by the equations¹⁸

$$N_i = \frac{2m_{d2}k_B T}{\pi \hbar^2} \ln \left[1 + \exp \left(\frac{E_F - E_i}{k_B T} \right) \right], \quad (3.1)$$

$$N'_i = \frac{4m_{d4}k_B T}{\pi \hbar^2} \ln \left[1 + \exp \left(\frac{E_F - E'_i}{k_B T} \right) \right], \quad (3.2)$$

where N_i and N'_i are the electron concentrations of the i th subband in the two- and fourfold valleys, respectively, m_{d2} and m_{d4} are the density-of-state effective masses in the respective valleys, E_i and E'_i are the subband energies for the two- and fourfold valleys, respectively, E_F is the Fermi energy level, and k_B is the Boltzmann constant. The resultant subband energy difference (Fig. 4) suggests that more electrons should occupy the high valley of the (110) surface (the twofold valley) than that of the (100) surface (the fourfold valley). However, as shown in Fig. 5, the difference in the electron occupancy between the low and high valleys is larger in (110) UTB SOI *n*-MOSFETs than in the (100). In the (100) UTB SOI *n*-MOSFETs, the subband energy split leads to carrier repopulation from the fourfold valley [the high valley in (100)] to the twofold valley [the low valley in

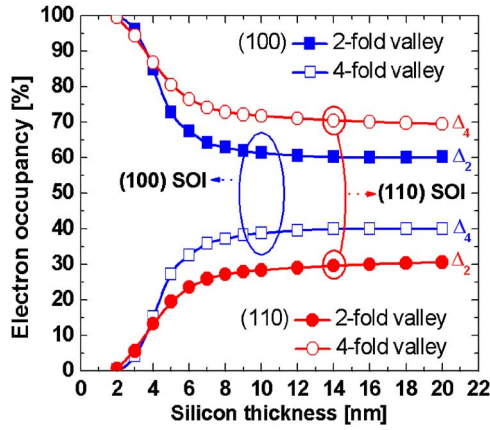


FIG. 5. (Color online) Electron occupancy of each valley as a function of top silicon thickness in (110) and (100) UTB SOI n -MOSFETs at E_{eff} of 0.116 MV/cm.

(100)]. This is due to the exponential term in Eqs. (3.1) and (3.2). On the other hand, the valley degeneracy factor in (110) UTB SOI n -MOSFETs is more prominent than a lesser subband energy split. However, although carriers in the low valley seem to easily jump into the high valley, the electron occupancy is more strongly influenced by the valley degeneracy factor of the fourfold valley, which is twice that of the twofold valley, than by the small subband split. Consequently, the electron occupancy of the low valley in (110) UTB SOI n -MOSFETs is higher than that in (100). Figure 6 shows the electron mobility of (110) SOI n -MOSFETs in each valley. Since the electron occupancy of the fourfold valley is higher than that of the twofold valley, the total mobility depends on the fourfold valley mobility. Although almost all electrons occupy the fourfold valley, where the conductivity effective mass is less than in the twofold valley of the (110) surface, the electron mobility decreases with the top silicon thickness. This indicates that a decrease in intervalley phonon scattering is not sufficiently effective in increasing the mobility on the (110) surface. Since the conductivity effective mass (m_c) of the fourfold valley is less than that of the twofold valley in (110), the higher occupancy in the low valley should increase the total mobility. However, we found no mobility enhancement in the thickness range around 5 nm for (110) UTB SOI n -MOSFETs, in contrast to

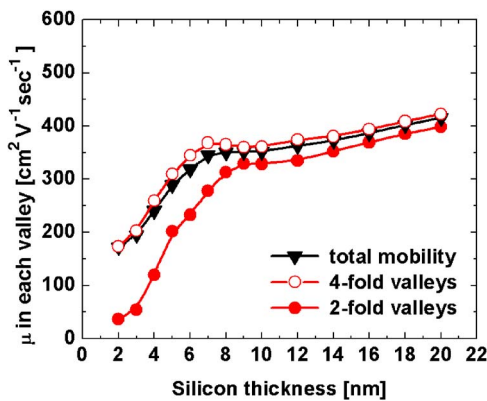


FIG. 6. (Color online) Electron mobility in each valley as a function of top silicon thickness in (110) UTB SOI n -MOSFETs at E_{eff} of 0.116 MV/cm.

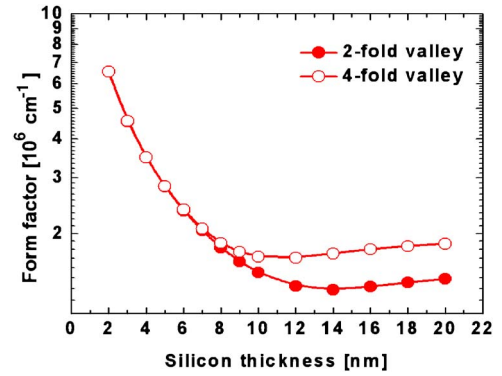


FIG. 7. (Color online) Form factor of each valley as a function of top silicon thickness in (110) UTB SOI n -MOSFETs at E_{eff} of 0.116 MV/cm.

(100) UTB SOI n -MOSFETs, even though the occupancy of the low valley was higher in the (110) UTB SOI n -MOSFETs than in (100). In such nanoscale-thickness SOI n -MOSFETs, it would be expected that most electrons occupy the lowest energy valley in an inversion layer. In such a case, the mobility is mainly determined by intravalley acoustic phonon scattering according to the following equations:^{19,20}

$$\mu_{\text{ac}} = \frac{q}{m_c} \cdot \frac{\hbar^3 \rho s_l^2}{m_d n_v D_{\text{ac}} k_B T} \cdot \frac{1}{W}, \quad (3.3)$$

$$W = \left(\int |\psi(z)|^4 dz \right)^{-1}, \quad (3.4)$$

where q is the elementary charge, \hbar is Planck's constant over 2π , k_B is the Boltzmann constant, ρ is crystal density, s_l is sound velocity, D_{ac} is acoustic deformation potential, n_v is a valley degenerate factor, m_c and m_d are conductivity effective mass and density-of-state effective mass, respectively, ψ is the lowest subband envelope function, and W is a form factor.

The inverse of W in Eq. (3.3) is the effective width of the inversion layer, and the electron mobility limited by intravalley acoustic phonons is dependent on it. The degradation of the electron mobility in (110) UTB SOI n -MOSFETs can be explained by the dramatic increase of the form factor, indicating a decrease in the effective width of the inversion layer. Figure 7 shows simulation results for the form factor in (110) UTB SOI n -MOSFETs as a function of the top silicon thickness. The form factor of the twofold valley increased with decreasing top silicon thickness below 12 nm and that of fourfold valley increased below 10 nm. The increase of the form factor in each valley resulted in a decrease in the total mobility. The subband energy split and the form factor compete with each other; i.e., the former increases the mobility but the latter decreases it. Thus, in (110) UTB SOI n -MOSFETs, the mobility would be mainly limited by the form factor since the subband energy split in the (110) surface is lower than that in the (100) surface.

To confirm our simulation results, we compared them with the experimental data of Tsutui *et al.*¹⁴ (Fig. 8). The differences in the mobility values between our simulation and experimental data can be attributed to our simulation

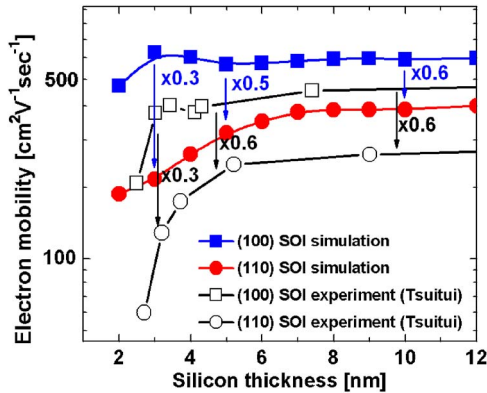


FIG. 8. (Color online) Comparison between simulation and experiment results: the simulation results were obtained at E_{eff} of 0.116 MV/cm, and the experiment results were acquired by Tsuitui *et al.* (Ref. 14) at N_{inv} of $6 \times 10^{12} \text{ cm}^{-2}$.

ignoring other scattering mechanisms apart from the phonon scattering. However, the trend of the mobility dependence on the top silicon thickness from the simulation was consistent with the experimental results for both (110) and (100) SOI *n*-MOSFETs. The mobility degradation ratio between the (110) and (100) SOI *n*-MOSFETs increased in the silicon thickness range below 5 nm in both the simulation and the experimental results. For example, the mobility of a (110) SOI *n*-MOSFET at thicknesses of 10 and 3 nm was 60% and 30% of that for (100) SOI *n*-MOSFET, respectively. Regarding why no mobility enhancement at top silicon thickness of about 5 nm was observed in (110) UTB SOI *n*-MOSFETs, we offer a reason different from that given by Tsuitui *et al.*¹⁴ They explained that the lack of mobility enhancement associated with less carrier repopulation between the two- and fourfold valleys, less suppression of intervalley phonon scattering, and δt_{SOI} -induced scattering.²¹ However, we found that the separation of the electron occupancy between the low valley (110: fourfold valley, 100: twofold valley) and the high valley (110: twofold valley, 100: fourfold valley) is greater in (110) UTB SOI *n*-MOSFETs than in (100), as shown Fig. 5. As a result, carrier repopulation—the main cause of the electron mobility enhancement in (100) UTB SOI *n*-MOSFETs—occurs to a greater degree in (110) UTB SOI *n*-MOSFETs than in (100) UTB SOI *n*-MOSFETs. Despite the higher carrier repopulation in (110) UTB SOI *n*-MOSFETs, the electron mobility when the top silicon thickness is about 5 nm is reduced rather than enhanced because the inversion width is physically restricted when the thickness is less than 10 nm. Therefore, we speculate that the decrease in the electron mobility as the top silicon layer in (110) UTB SOI *n*-MOSFETs becomes thinner is mainly associated with increased intravalley scattering as the top silicon decreases (Fig. 6).

IV. CONCLUSION

We investigated the electron mobility behavior in (110) UTB SOI *n*-MOSFETs through theoretical simulation, comparing it to that in (100) UTB SOI *n*-MOSFETs. The results indicated that the electron mobility in (110) UTB SOI *n*-MOSFETs decreases with the top silicon thickness, unlike

that in (100) UTB SOI *n*-MOSFETs (i.e., there is no electron mobility enhancement), resulting in a more significant mobility decrease than that of (100). We confirmed that the mobility degradation between (110) and (100) UTB SOI *n*-MOSFETs as a function of top silicon thickness is consistent with previously reported experimental data. We also found that although the low-valley electron population in (110) SOI is greater than that in (100) UTB SOI *n*-MOSFETs, the electron mobility decreases with the top silicon thickness. This difference in the mobility behavior between (110) and (100) UTB SOI *n*-MOSFETs is probably attributable to the form factor, which is mainly determined by intravalley scattering, rather than the subband energy split.

ACKNOWLEDGMENTS

This work was supported by the Brain Korea 21 Project in 2007. We are also indebted to Ji-Young Baek and Yong-Seon Lee for helpful discussions.

- ¹M. Yoshimi, T. Wada, K. Kato, and H. Tango, Tech. Dig. - Int. Electron Devices Meet. **1987**, 640.
- ²E. Suzuki, K. Ishii, S. Kanemaru, T. Maeda, T. Tsutsumi, T. Sekigawa, K. Nagai, and H. Hiroshima, IEEE Trans. Electron Devices **47**, 354 (2000).
- ³S. Takagi, A. Toriumi, M. Iwase, and H. Tango, IEEE Trans. Electron Devices **41**, 2357 (1994).
- ⁴Y.-K. Choi, K. Asano, N. Lindert, V. Subramanian, T.-J. King, J. Bokor, and C. Hu, Tech. Dig. - Int. Electron Devices Meet. **1999**, 919.
- ⁵K. Uchida, H. Watanabe, A. Kinoshita, J. Koga, T. Numata, and S. Takagi, Tech. Dig. - Int. Electron Devices Meet. **2002**, 47.
- ⁶S. Takagi, J. Koga, and A. Toriumi, Jpn. J. Appl. Phys., Part 1 **37**, 1289 (1998).
- ⁷O. Weber, F. Ducroquet, T. Ernst, F. Andrieu, J.-F. Damlencourt, J.-M. Hartmann, B. Guillaumot, A.-M. Papon, H. Dansas, L. Brévard, A. Toffoli, P. Besson, F. Martin, Y. Morand, and S. Deleonibus, Symp. VLSI Technol., Dig. Tech. Pap. **2004**, 42.
- ⁸J.-S. Goo, Q. Xiang, Y. Takamura, H. Wang, J. Pan, F. Arasnia, E. N. Paton, P. Besser, M. V. Sidorov, E. Adem, A. Lochtefeld, G. Braithwaite, M. T. Currie, R. Hammond, M. T. Bulsara, and M.-R. Lin, IEEE Electron Device Lett. **24**, 351 (2003).
- ⁹J. G. Park, T. H. Shim, T. H. Lee, Y. K. Park, H. K. Moon, S. L. Maeng, W. J. Cho, and S. D. Yoo, IEEE Int. SOI Conf. Proc. **2003**, 61.
- ¹⁰M. Yang, M. Jeong, L. Shi, K. Chan, V. Chan, A. Chou, E. Gusev, K. Jenkins, D. Boyd, Y. Ninomiya, D. Pendleton, Y. Surpris, D. Heenan, J. Ott, K. Guarini, C. D'Emic, M. Cobb, P. Mooney, B. To, N. Rovedo, J. Benedict, R. Mo, and H. Ng, Tech. Dig. - Int. Electron Devices Meet. **2003**, 453.
- ¹¹M. L. Lee, C. W. Leitz, Z. Cheng, A. J. Pitera, T. Langdo, M. T. Currie, G. Taraschi, E. A. Fitzgerald, and D. A. Antoniadis, Appl. Phys. Lett. **79**, 3344 (2001).
- ¹²A. Shimizu, K. Hachimine, N. Ohki, H. Ohta, M. Koguchi, Y. Nonaka, H. Sato, and F. Ootsuka, Tech. Dig. - Int. Electron Devices Meet. **2001**, 433.
- ¹³C.-H. Ge, C.-C. Lin, C.-H. Ko, C.-C. Huang, Y.-C. Huang, B.-W. Chan, B.-C. Perng, C.-C. Sheu, P.-Y. Tsai, L.-G. Yao, C.-L. Wu, T.-L. Lee, C.-J. Chen, C.-T. Wang, S.-C. Lin, Y.-C. Yeo, and C. Hu, Tech. Dig. - Int. Electron Devices Meet. **2003**, 73.
- ¹⁴G. Tsuitui and T. Hiramoto, IEEE Trans. Electron Devices **53**, 2582 (2006).
- ¹⁵H. Ezawa, S. Kawaji, and K. Nakamura, Jpn. J. Appl. Phys. **13**, 126 (1974).
- ¹⁶SILVACO International, ATLAS User's Manual, 2006.
- ¹⁷F. Stern, Phys. Rev. B **5**, 4891 (1972).
- ¹⁸S. Takagi, J. Hoyt, J. J. Welsler, and J. Gibbons, J. Appl. Phys. **80**, 1567 (1996).
- ¹⁹S. Takagi, A. Toriumi, M. Iwase, and H. Tango, IEEE Trans. Electron Devices **41**, 2363 (1994).
- ²⁰K. Masaki, C. Hamaguchi, K. Taniguchi, and M. Iwase, Jpn. J. Appl. Phys., Part 1 **28**, 1856 (1989).
- ²¹K. Uchida and S. Takagi, Appl. Phys. Lett. **82**, 2916 (2003).

Journal of Applied Physics is copyrighted by the American Institute of Physics (AIP).
Redistribution of journal material is subject to the AIP online journal license and/or AIP
copyright. For more information, see <http://ojps.aip.org/japo/japcr/jsp>